Spontaneous chiral symmetry breaking in collective active motion

Rebekka E. Breier, Robin L. B. Selinger, Giovanni Ciccotti, Stephan Herminghaus, and Marco G. Mazza

Phys. Rev. E **93**, 022410 — Published 18 February 2016

DOI: 10.1103/PhysRevE.93.022410

Spontaneous chiral symmetry breaking in collective active motion

Rebekka E. Breier,[1] Robin L. B. Selinger,[2] Giovanni Ciccotti,[3,4] Stephan Herminghaus,[1] and Marco G. Mazza[1,*]

[1] *Max Planck Institute for Dynamics and Self-Organization (MPIDS), Am Fassberg 17, 37077 Göttingen, Germany*
[2] *Chemical Physics Interdisciplinary Program, Liquid Crystal Institute, Kent State University, Kent, OH, USA*
[3] *Department of Physics, University of Rome "La Sapienza", P.le A. Moro 5, 00185 Rome, Italy*
[4] *School of Physics, University College Dublin, Belfield, Dublin 4, Ireland*

Chiral symmetry breaking is ubiquitous in biological systems, from DNA to bacterial suspensions. A key unresolved problem is how chiral structures may spontaneously emerge from achiral interactions. We study a simple model of active swimmers in three dimensions that effectively incorporates hydrodynamic interactions. We perform large-scale molecular dynamics simulations (up to 10^6 particles) and find long-lived metastable collective states that exhibit chiral organization although the interactions are achiral. We elucidate under which conditions these chiral states will emerge and grow to large scales. To explore the complex phase space available to the system, we perform nonequilibrium quenches on a one dimensional Lebwohl–Lasher model with periodic boundary conditions to study the likelihood of formation of chiral structures.

PACS numbers: 47.54.-r, 05.65.+b, 87.18.Gh, 87.18.Hf

The study of collective phases of organization of self-propelled particles (SPP) has attracted considerable interest in recent years. This behavior is found in a remarkable range of different scales: from microtubules and molecular motors inside a cell [1], to bacteria forming vortices [2, 3], and to flocks of birds such as starling's spectacular shapes in the evening sky [4–6], to schools of fish [7] and herds of wildebeest. The seminal work of Vicsek *et al.* [8] ushered the study of collective motion of active particles into the realm of statistical physics. A multitude of different states and nonequilibrium transitions have been found in different models of collective behavior [9–13] that exhibit ferromagnetic or nematic symmetry.

An intriguing behavior is the emergence of chirality. Bacterial suspensions show striking examples of chiral behavior [3, 14, 15]; colonies of the amoeba *Dictyostelium discoideum* aggregate in swirling localized vortices [16, 17]. Chiral swimmers exhibit helical paths robust in the presence of fluctuations [18], and rotationally driven spinners self-organize in into rotating crystals [19]. Spontaneous swarm rotation was found in [20–22]. The emergence of biological structures at the beginning of life that spontaneously break chiral symmetry has no clear explanation yet [23–25].

Here, we show that a simple model of SPP with achiral interactions may exhibit a chiral symmetry breaking under certain boundary conditions. We investigate the conditions which favor the formation of long-lived, metastable chiral pattern from an isotropic state. Finally, to explore the vast phase space available to the SPP we perform nonequilibrium quenches on the Lebwohl–Lasher interaction potential for a one-dimensional chain. We find that chiral structures become likely for large enough systems.

* Corresponding author: marco.mazza@ds.mpg.de

We model active particles through simple interactions among SPP that effectively mimic the active motion of bacteria. The SPP are modeled as point particles moving in the direction of their intrinsic orientation $\hat{e}_i$. It is a common choice to choose a constant speed v_0 because at small Reynolds numbers rapid fluctuations of the speed are exponentially damped. Aiming for a simple model system, we choose a nematic interaction that has head-tail symmetry. Nematic interactions represent to leading order the effective hydrodynamic interactions among bacteria [26]. Our model captures the hydrodynamic interactions in a minimal way. However, their role is still a matter of debate. For example, experimental measurements of the flow field generated by *Escherichia coli* show that the effects of hydrodynamic interactions are washed out by the stochasticity of the dynamics [27]. The equations of motion for particle i read

$$\dot{\vec{r}}_i = v_0 \hat{e}_i \,, \tag{1a}$$

$$\dot{\hat{e}}_i = -\gamma \frac{\partial U}{\partial \hat{e}_i} + \vec{\xi}_i(t) \tag{1b}$$

where $\vec{r}_i$ and $\hat{e}_i$ are the position and direction, respectively, of the i-th particle, such that $|\hat{e}_i|^2 = 1$ and $\hat{e}_i \cdot \dot{\hat{e}}_i = 0$ at all times. The noise $\vec{\xi}(t)$ is a uniformly distributed vector on the surface of a sphere [28] with $\langle \xi_i(t)\xi_j(t')\rangle = 2D_r\delta(t-t')\delta_{ij}$, where $D_r = \eta^2/\gamma$. $U = -\frac{1}{2}\sum_{i=1}^{N}\frac{1}{n_i}\sum_{j\in n_i}(\hat{e}_i\cdot\hat{e}_j)^2$ is the Lebwohl–Lasher potential that induces nematic alignment [29], where the second sum extends to the n_i neighbors of particle i within a sphere of radius ϵ. A similar potential has been studied in two spatial dimensions by a number of authors [8, 9, 12, 13], however, past work has focused on the limit of fast angular relaxation which leads to finite-difference equations. Instead, we explicitly solve Eq. (1) leaving γ as an explicit parameter.

We perform molecular dynamics simulations of a three-dimensional system with up to $N = 10^6$ particles in a cubic box of volume $V = L^3$. We employ an explicit

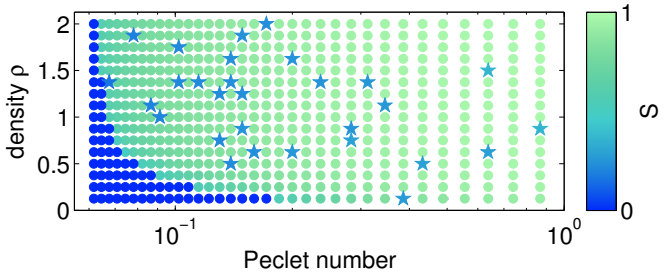

Figure 1. (Color online) Phase diagram of the system of self-propelled particles in terms of Péclet number $\mathcal{P}$ and density ρ. The color indicates the global nematic order parameter and shows the regions of the nematic and the isotropic phases (denoted by •). The symbol ★ indicates a chiral pattern which developed in one specific simulation run and can arise everywhere in the nematic region of the phase diagram.

Euler algorithm with time-step $\delta t = 0.1$ for the translational and orientational dynamics, where to satisfy the constraints on $\hat{e}_i$ we use the algorithm of [30–32]. We implement an efficient neighbor search [33, 34] that allows us to reach large system sizes, and we apply the usual periodic boundary conditions in all three dimensions. The reason for using periodic boundaries is that we aim to study the role of fluctuations in an active system without the influence of external fields (such as confining walls).

All following results are shown for $N = 66^3$, $v_0 = 0.5$, and $\gamma = 0.1$. The interaction range sets the length scale in our system ($\epsilon = 1$).

To quantify the degree of nematic alignment we consider the nematic order parameter S defined as the largest eigenvalue of the nematic order tensor $\mathbf{Q} = \frac{1}{2N}\sum_{i=1}^{N}[3\hat{e}_i \otimes \hat{e}_i - \mathbf{I}]$ where $\otimes$ is the tensor product. The nematic director $\hat{d}$ is defined as the eigenvector associated to S. The local director $\hat{d}^{\rm loc}$ is accordingly defined by replacing all N particles in the definition of $\mathbf{Q}$ with a subset of N_α particles (e.g., contained in a layer of finite thickness).

Figure 1 shows the nonequilibrium phase diagram of the system presented in terms of particle density $\rho = N/V$ and Péclet number

$$\mathcal{P} \equiv \frac{\text{advection}}{\text{diffusion}} = \frac{\epsilon v_0}{\epsilon^2\eta^2/\gamma} = \frac{v_0\gamma}{\epsilon\eta^2}\,, \qquad (2)$$

which are useful to characterize bacterial or algal suspensions [35]. There we have also reported the points where a chiral pattern has spontaneously developed. At sufficiently large $\mathcal{P}$, the system is in the nematic state independently of ρ with $S \in [0.5, 1]$. Moreover, as observed in [13] (but in 2D), the system's steady-state is spatially homogeneous with sub-populations moving in opposite directions. As $\mathcal{P}$ decreases there is a clear transition to a spatially homogeneous, isotropic state.

In the region of the phase diagram where $\mathcal{P}$ and S are large, the system may also develop states where there is no single, global nematic director, but rather $\hat{d}^{\rm loc}$ rotates in space forming a helical structure. Figure 2 shows four cross-sections of the system equally spaced along the helical axis. The particles contained in each of these cross-sections of width $\delta \approx 1.1\epsilon$ still preserve nematic ordering with a well-defined $\hat{d}^{\rm loc}$. As one moves along the helical axis this local nematic director slowly rotates with a constant twist angle. We show in Fig. 3(a) how the components of $\hat{d}^{\rm loc}$ vary along the helical axis (conventionally called x-axis). The profiles of the y and z components of the director are very well fit by sinusoidal functions, as expected for helical structures. The axis of the helix is in most cases, like in this example, parallel to one of the box edges with the pitch being $2L$ due to the periodic boundary conditions together with the nematic interactions. However, the helix can also be found at an angle with the box edge (e.g., along one of the diagonals, with the pitch adjusted accordingly). We observe left- and right-handed helices with equal probability, and, additionally, once a chiral state is formed it is metastable at least up to 2×10^6 time steps.

The formation of a chiral structure in the SPP model is not determined by the initial conditions. Starting from the same initial conditions (positions and directions of all particles), different realizations (different random seeds) can lead to a nematic, or a left- or right-handed chiral structure. We also tested the effect of different random number generators on the stability and reproducibility of the chiral state including a Mersenne twister algorithm [36]. Both the structure of a single chiral configuration (homogeneous director twist, pitch of twice the box size) as well as the overall occurrence in the phase diagram and long-lived metastability remained the same

To characterize a chiral state a pseudoscalar order parameter is useful. The simplest combination of orientations and distances that provides a pseudoscalar is $(\hat{e}_i \times \hat{e}_j) \cdot (\vec{r}_i - \vec{r}_j)$ [37]. We define the chiral order parameter averaged over all particles as

$$S_\chi = -\frac{\pi^3}{6(4-\pi)}\frac{1}{N}\sum_{i=1}^{N}\frac{1}{N_i}\sum_{j=1}^{N_i}\left[(\hat{e}_i \times \hat{e}_j)\cdot\frac{\vec{r}_{ij}}{|\vec{r}_{ij}|}\right](\hat{e}_i \cdot \hat{e}_j) \qquad (3)$$

where $\vec{r}_{ij} \equiv \vec{r}_i - \vec{r}_j$ and the sum over j includes all N_i particles in a sphere centered on $\vec{r}_i$ with radius $L/4$. We note that the normalization depends on the radius (here $L/4$) which defines the volume over which the local average (all N_i particles) is taken. The normalization is calculated analytically for an ideal chiral configuration with $\hat{e} = \pm(\cos(z\pi/L), \sin(z\pi/L), 0)$ S_χ is a pseudoscalar symmetric for $\hat{e}_i \to -\hat{e}_i$ and vanishes in both the nematic and the isotropic case. It is normalized so that $S_\chi = +1(-1)$ indicates a left-handed (right-handed) chiral structure. Figure 3(b) shows a typical evolution of S_χ.

An estimate for the probability of the formation of a chiral pattern from 300 independent simulations for different values of $\mathcal{P}$ is shown in Table I. Although the statistics is limited, this probability exhibits a maximum for $\mathcal{P} = 0.10$. $\langle|S_\chi|\rangle_\chi$ increases as the Péclet number increases. The reason is the same as for the increase of S with increasing $\mathcal{P}$ (Fig. 1): Because the system has

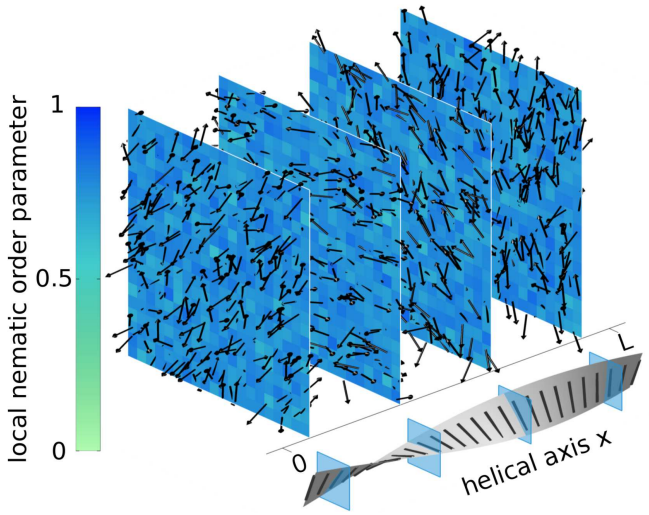

Figure 2. (Color online) Cross-sections of a typical chiral configuration ($\rho = 1.625, \mathcal{P} = 0.08$). The color code represents the local nematic order parameter and the arrows represent the SPP. The ribbon in the bottom shows the helicoidal behavior of $\hat{d}^{\rm loc}$ in different cross-sections.

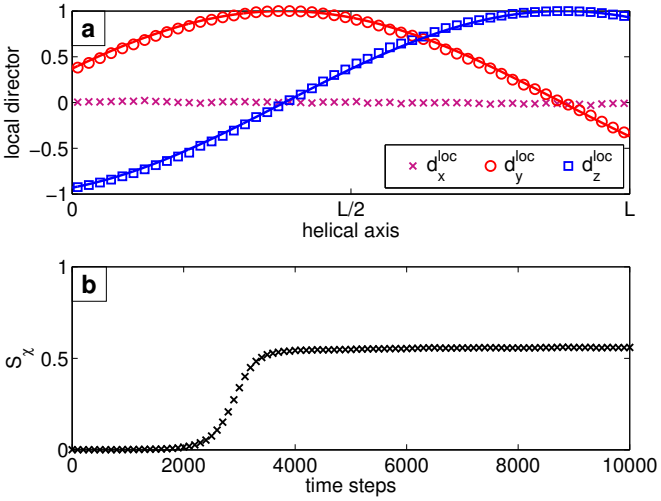

Figure 3. (Color online) (a) Components of $\hat{d}^{\rm loc}$ along the helical axis ($\hat{x}$) of the chiral pattern (see Fig. 2). The symbols are the components of $\hat{d}^{\rm loc}$ (in slices normal to the helical axis) and the solid lines are sinusoidal least square fits $d^{\rm loc}_{y,z} = \cos(\pi x/L + \phi_{y,z})$. (b) Time evolution of the chiral order parameter for the same simulation. The transient evolution before reaching the steady state can extend up to 10^4 time steps

smaller orientational fluctuations for large $\mathcal{P}$, both order parameters increase.

We now turn to the study of the formation and stability of the chiral structure. We consider the local deformations of a nematic fluid. The demonstration that there are only three elementary deformations of the equilibrium nematic director field $\hat{d}$ can be found in the book by P. G. de Gennes and J. Prost [38], and these are: splay $(\nabla\cdot\hat{d})^2$,

$\mathcal{P}$	$P(\lvert S_\chi\rvert > 0.2)$	$\langle\lvert S_\chi\rvert\rangle_\chi$
0.08	3.3%	0.48
0.10	6.7%	0.64
0.14	5.7%	0.74
0.20	4.0%	0.82

Table I. Probability $P(|S_\chi| > 0.2)$ of the formation of a chiral structure for different Péclet numbers (300 independent simulations each, $\rho = 1$). $\langle|S_\chi|\rangle_\chi$ denotes the mean of the absolute chiral order parameter conditional to the simulations resulting in a chiral structure with the helical axis parallel to the box edge.

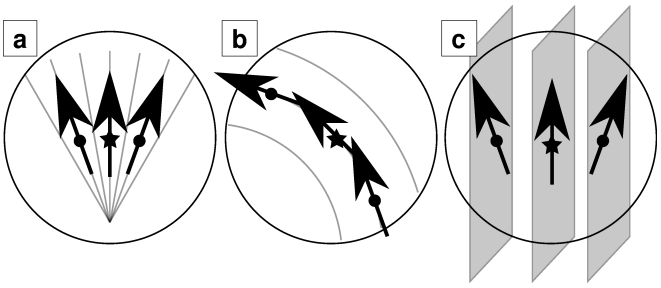

Figure 4. Ideal splay (a), bend (b), and twist (c) deformations of the director field. The reference particle (★) does not experience any torque from the neighboring particles (•).

bend $[\hat{d}\times(\nabla\times\hat{d})]^2$, and twist $[\hat{d}\cdot(\nabla\times\hat{d})]^2$ [38]. For ideal splay, bend or twist deformations the total torque on a reference particle vanishes (Fig. 4). However, the splay deformation is not stable in the SPP system because the system does not have sinks or sources. The bend deformation does not persist because there is no centrifugal force that would keep the particles on a curved path. On the other hand, the SPP in an ideal twist deformation move within nematically ordered slices and therefore the deformation persists. Thus, due to symmetry, the twist pattern is the only one which is invariant under the motion of active particles.

Next, we show how an achiral (nematic) interaction can lead to a chiral pattern by investigating the evolution of an isotropic to a chiral state in a simulation with large $\mathcal{P}$. The interaction of the SPP leads to local alignment. Firstly, areas of high local alignment grow with time. As these areas have grown to a certain size, they typically form a planar domain with $\hat{d}^{\rm loc}$ perpendicular to the layer normal (Fig. 5(a)). Secondly, in the evolution of the chiral state, we typically find two of these areas which fill almost the entire box and have a specific geometrical relation: the two planes have to be parallel and the two $\hat{d}^{\rm loc}$ form an angle close to $\pi/2$. Domains with different $\hat{d}^{\rm loc}$ start competing and that can result in a chiral structure. Only long wavelength fluctuations can untwist a chiral configuration. An example of the formation of these planes is shown in Fig. 5(b-c). It is quite simple to identify distinct and differently oriented

domains that drive the formation of a chiral structure. We show the temporal evolution of domains with different orientations for a chiral structure (Fig. 5(d)) and also for a system that eventually evolves into a nematic state (Fig. 5(e)).

Seeding the system with two planar, ordered domains increases the probability of the chiral state (for a given $\mathcal{P}$) from roughly few percent to about 50%. This shows that the seeds are a good prerequisite for the chiral state but also that the fluctuations must play a key role since the probability does not reach 100%. Below, we elucidate the role of fluctuations in the driving mechanism.

Nonequilibrium systems have access to much more states than their equilibrium counterparts because detailed balance is absent. It would then be very useful to devise a way to explore this complex phase space and study the relative probabilities to transition from one state to the other. In an attempt to do so, and to gain insight into the statistics of the observed chiral states, we consider that the velocity orientation of the system is governed by the Lebwohl–Lasher potential function in Eq. (1b). To understand the resulting statistics and dependence on system size, we carry out simulations of a 1D chain of N Lebwohl–Lasher spins with periodic boundary conditions under a nonequilibrium rapid quench. We rewrite the potential for convenience as $V = -\sum_{i=1}^{N} J\cos\left[2(\theta_{i+1}-\theta_i)\right]$. The system is not in thermal equilibrium; rather, the local velocity orientation evolves via a rapid quench from a disordered state to one with strong local orientational correlations and significant variation along only one dimension. We model each spin's motion using the velocity Verlet method with a Langevin thermostat, annealing rapidly from $T = 10$ to $T = 10^{-7}$ in 6×10^5 time steps, with 200 annealing trials for each chain length N.

Surprisingly, we find that the most likely final state for chains with $N \geqslant 200$ is a metastable state with exactly one twist of either $\pm\pi$, while for shorter chains the most likely final state is untwisted, as shown in Fig. 6. To explain this result, we consider the energy landscape of the 1D Lebwohl–Lasher model. The potential energy associated with a state with n half-twists is $2J(n\pi/N)^2$ [39] and these twisted states are separated by significant energy barriers. In quenching the system from a random initial state to low temperature, instead of finding the untwisted ground state, the system may easily become stuck in a twisted metastable state. It is interesting to note that for the related *equilibrium* 1D Lebwohl–Lasher model at any finite temperature, the state with exactly one half twist (positive or negative) has the highest fugacity for long enough chains. For shorter chains, by contrast, the untwisted ground state has the highest fugacity in the equilibrium system. Though our 1D Lebwohl–Lasher model simulations are not in thermal equilibrium, the rapid quench to low temperature through the energy landscape shows similar behavior, with long chains $N \geqslant 200$ showing highest probability to form a single half-twist while shorter chains' most probable final state is the untwisted ground state. We also find that the mean square number of twists $\langle n^2\rangle$ in our rapidly quenched 1D Lebwohl–Lasher simulations increases linearly with chain length N, indicating that variation in velocity orientation follows random walk statistics. A very similar behavior is found in the SPP model when a simulation box of aspect ratio $10:1:1$ is used ($N = 10\times23^3$, $\rho = 1$, $\mathcal{P} = 0.08$). The probability of forming a chiral structure with twists of $\pm\pi$ is six times larger than for a cubic box. Moreover, we also observe the spontaneous formation of structures with a twist of $\pm2\pi$ in the elongated box.

A finite-size scaling analysis of the SPP model would be computationally very expensive. But by studying the Lebwohl–Lasher potential energy we can gain insight into the complex phase space that underlies the SPP twist dynamics. The combined results point to the fact that as the system size increases, the relevance of the twist states too increases.

In summary, we have shown that a model of SPP with achiral interactions can exhibit a spontaneous chiral symmetry breaking and that orientational fluctuations play a key role in the emergence of chiral structures. From our molecular dynamics simulations we always find that splay and bend are not stable for long times; only twist is. We have verified that our results are robust by studying systems of different size, and no qualitative difference was found. Moreover, by performing nonequilibrium quenches on the Lebwohl–Lasher model with periodic boundary conditions we have studied the likelihood of formation of chiral structures. A coarse-graining of the equations of motion would provide further insight into the problem. This is left for future work.

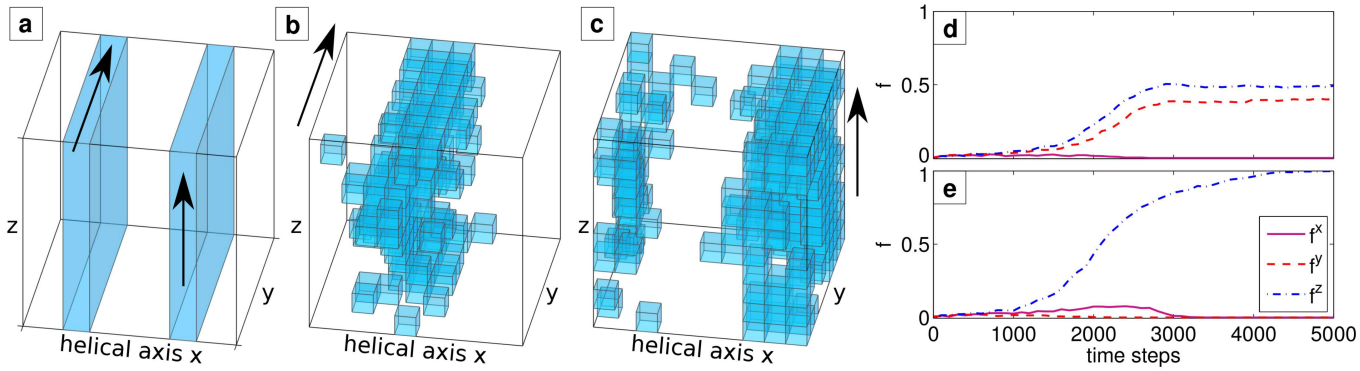

Figure 5. (Color online) Formation of the chiral pattern. (a) Sketch of two competing layers (each nematically aligned). Here, the angle between the two $\hat{d}^{\rm loc}$ is $\pi/2$. (b) and (c) Example from the same simulation as in Figs. 2 and 3 at time $t = 2000$ time steps. The system is divided into 10^3 boxes in each of which the fraction $f_{\rm box}^{\{y,z\}}$ of particles with $|e_y| > 0.9$ (b) and $|e_z| > 0.9$ (c) is determined. Only boxes with $f_{\rm box}^{\{y,z\}} > 0.15$ are plotted. $f_{\rm box}^{x}$ can be defined accordingly. (d) and (e) Evolution of the fraction $f^{\{x,y,z\}}$ of boxes with $f_{\rm box}^{\{x,y,z\}} > 0.15$ for the same chiral simulation (d) and a nematic example (e). The chiral structure shows two growing domains of similar size and different orientations, while only one orientation dominates in the nematic case.

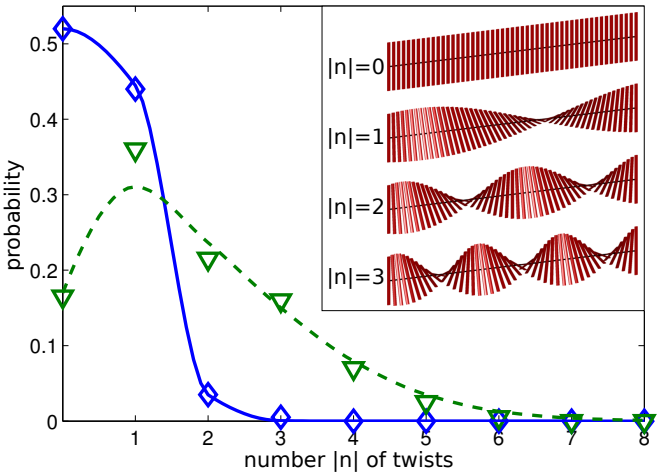

Figure 6. (Color online) Inset: When annealed, the 1D nematic rotor model can evolve into the untwisted ground state or a chiral metastable state with $\pm n$ twists. Main panel: Frequency of final states has a maximum value at $|n| = 1$ for a long chain with $N = 800$ (green $\triangledown$, fit as green dashed line), and at $|n| = 0$ for a short chain with $N = 100$ (blue $\diamondsuit$, fit as blue solid line). The lines are guides for the eye.

[1] F. J. Ndlec, T. Surrey, A. C. Maggs, and S. Leibler, Nature **389**, 305 (1997).

[2] H. H. Wensink, J. Dunkel, S. Heidenreich, K. Drescher, R. E. Goldstein, H. Löwen, and J. M. Yeomans, Proc. Natl. Acad. Sci. USA **109**, 14308 (2012).

[3] H. Wioland, F. G. Woodhouse, J. Dunkel, J. O. Kessler, and R. E. Goldstein, Phys. Rev. Lett. **110**, 268102 (2013).

[4] M. Ballerini, N. Cabibbo, R. Candelier, A. Cavagna, E. Cisbani, I. Giardina, V. Lecomte, A. Orlandi, G. Parisi, A. Procaccini, M. Viale, and Z. Zdravkovic, Proc. Natl. Acad. Sci. USA **105**, 1232 (2008).

[5] A. Cavagna, A. Cimarelli, I. Giardina, G. Parisi, R. Santagati, F. Stefanini, and M. Viale, Proc. Natl. Acad. Sci. USA **107**, 11865 (2010).

[6] A. Attanasi, A. Cavagna, L. Del Castello, I. Giardina, T. S. Grigera, A. Jelić, S. Melillo, L. Parisi, O. Pohl, E. Shen, and M. Viale, Nat. Phys. **10**, 691 (2014).

[7] Y. Katz, K. Tunstrøm, C. C. Ioannou, C. Huepe, and I. D. Couzin, Proc. Natl. Acad. Sci. USA **108**, 18720 (2011).

[8] T. Vicsek, A. Czirók, E. Ben-Jacob, I. Cohen, and O. Shochet, Phys. Rev. Lett. **75**, 1226 (1995).

[9] G. Grégoire and H. Chaté, Phys. Rev. Lett. **92**, 025702 (2004).

[10] F. Peruani, A. Deutsch, and M. Bär, Phys. Rev. E **74**, 030904 (2006).

[11] H. Chaté, F. Ginelli, and R. Montagne, Phys. Rev. Lett. **96**, 180602 (2006).

[12] F. Peruani, A. Deutsch, and M. Bär, Eur. Phys. J. Spec. Top. **157**, 111 (2008).

[13] F. Ginelli, F. Peruani, M. Bär, and H. Chaté, Phys. Rev. Lett. **104**, 184502 (2010).

[14] E. Ben-Jacob, I. Cohen, O. Shochet, A. Tenenbaum, A. Czirók, and T. Vicsek, Phys. Rev. Lett. **75**, 2899 (1995).

[15] E. Lushi, H. Wioland, and R. E. Goldstein, PNAS **111**, 9733 (2014).

[16] A. Nicol, W. Rappel, H. Levine, and W. F. Loomis, J Cell Sci **112**, 3923 (1999).

[17] H. Levine, E. Ben-Jacob, I. Cohen, and W.-J. Rappel, in *45th IEEE Conference on Decision and Control* (2006) pp. 5073–5077.

[18] B. M. Friedrich and F. Jülicher, Phys. Rev. Lett. **103**, 068102 (2009).

[19] N. H. Nguyen, D. Klotsa, M. Engel, and S. C. Glotzer, Phys. Rev. Lett. **112**, 075701 (2014).

[20] U. Erdmann and W. Ebeling, Fluct. Noise Lett. **03**, L145 (2003).

[21] U. Erdmann, W. Ebeling, and A. S. Mikhailov, Phys. Rev. E **71**, 051904 (2005).

[22] J. Strefler, U. Erdmann, and L. Schimansky-Geier, Phys. Rev. E **78**, 031927 (2008).

[23] U. J. Meierhenrich, European Review **21**, 190 (2013).

[24] U. Meierhenrich, *Amino Acids and the Asymmetry of Life: Caught in the Act of Formation* (Springer, 2008).

[25] B. Nordén, J Mol Evol **11**, 313 (1978).

[26] A. Baskaran and M. C. Marchetti, PNAS **106**, 15567 (2009).

[27] K. Drescher, J. Dunkel, L. H. Cisneros, S. Ganguly, and R. E. Goldstein, PNAS **108**, 10940 (2011).

[28] A. Czirók, M. Vicsek, and T. Vicsek, Physica A: Statistical Mechanics and its Applications **264**, 299 (1999).

[29] P. A. Lebwohl and G. Lasher, Phys. Rev. A **6**, 426 (1972).

[30] K. Singer, A. Taylor, and J. V. L. Singer, Molecular Physics **33**, 1757 (1977).

[31] D. Fincham, CCP5 Quarterly **12**, 47 (1984).

[32] J. M. Ilnytskyi and M. R. Wilson, Computer physics communications **148**, 43 (2002).

[33] J. Boris, Journal of Computational Physics **66**, 1 (1986).

[34] S. Weinketz, Computer Physics Communications **74**, 228 (1993).

[35] R. Stocker and J. R. Seymour, Microbiol. Mol. Biol. Rev. **76**, 792 (2012).

[36] M. Matsumoto and T. Nishimura, ACM Trans. Model. Comput. Simul. **8**, 3 (1998).

[37] R. Memmer, Liquid Crystals **27**, 533 (2000).

[38] P.-G. de Gennes and J. Prost, *The Physics of Liquid Crystals* (Clarendon press, Oxford, 1993).

[39] $\Delta E_n = \langle -J\cos(2\Delta\theta)\rangle - E_0$ with $\Delta\theta = \frac{n\pi}{N}$ and $E_0 = -J$. The small-angle approximation $\cos(2\Delta\theta) \approx 1 - 2\Delta\theta^2$ leads to $\Delta E_n = 2J\left(\frac{n\pi}{N}\right)^2$.